3.2.2 Stabilisierung instabiler periodischer Orbits

Normalform einer subkrit. Hopf-Bif.:

$$\dot{z} = (\lambda + i\omega + (1+i\gamma)|z|^2)z + b\,(z(t-\tau) - z(t))$$

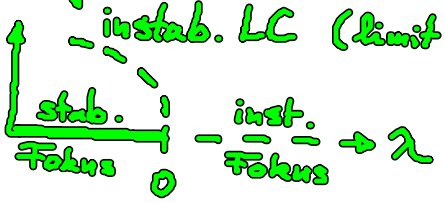

$\lambda < 0$, $\omega = 1$, $\gamma > 0$, $b = b_0 e^{i\beta} \in \mathbb{C}$

ohne Kontrolle

Odd-number orbit (= ungerade Zahl von reellen Floquet-Exp. > 0, hier $n = 1$; ohne „Torsion")

Nakajima (1997): Stabilisierung von odd-number orbits durch zeitverzögerte Rückkopplung nicht möglich („Odd-number Theorem")

Fiedler, Flunkert, Georgi, Hövel, Schöll, PRL 98, 114101 (2007)

„Odd-number Theorem" gilt nicht!

Laser exp. (Schikora et al. 2011)

Gegenbeispiel: subkrit. Hopf-Bifurkation (Orbit ohne Torsion!)
wähle b_0, β geeignet!

nichtinvasive Kontrolle: vgl. Kap. 1.3

wähle $\tau \overset{!}{=} nT = \frac{2\pi}{1-\gamma\lambda}$ (T = Periode des UPO, $n \in \mathbb{N}$)

unstable periodic orbit

(Pyragas-Kurve in der (τ, λ)-Ebene)

Hopf-Kurve: lin. Stab. des Fixp. $z(t) \sim e^{zt}$:

$$z + b(1 - e^{-z\tau}) = \lambda + i$$ vgl. 3.2.1

Hopf-Bif.: $z = i\omega$: $0 = \lambda + b_0[\cos(\beta - \omega\tau) - \cos\beta]$ (1)

$\omega - 1 = b_0[\sin(\beta - \omega\tau) - \sin\beta]$ (2)

(1) $\Rightarrow \omega\tau = \pm \arccos\left(\frac{b_0\cos\beta - \lambda}{b_0}\right) + \beta + 2\pi n$

$\left(\frac{b_0\cos\beta - \lambda}{b_0}\right)^2 = \cos(\beta - \omega\tau)^2$

$\left(\frac{\omega - 1 + b_0\sin\beta}{b_0}\right)^2 = \sin(\beta - \omega\tau)^2$

$\Big\} \cos^2 + \sin^2 = 1$

$\Rightarrow \omega = g(\lambda, b_0, \beta) \xrightarrow{\text{elim.}} \tau = h(\lambda, b_0, \beta)$

Hopf-Kurve in (τ, λ)

ohne Kontrolle ($b = 0$)

→ subkrit. Hopf

↳ – –

mit Kontrolle $b = b_0 e^{i\beta}$

↳ superkrit. Hopf

– – ↳ entlang der Pyragaskurve

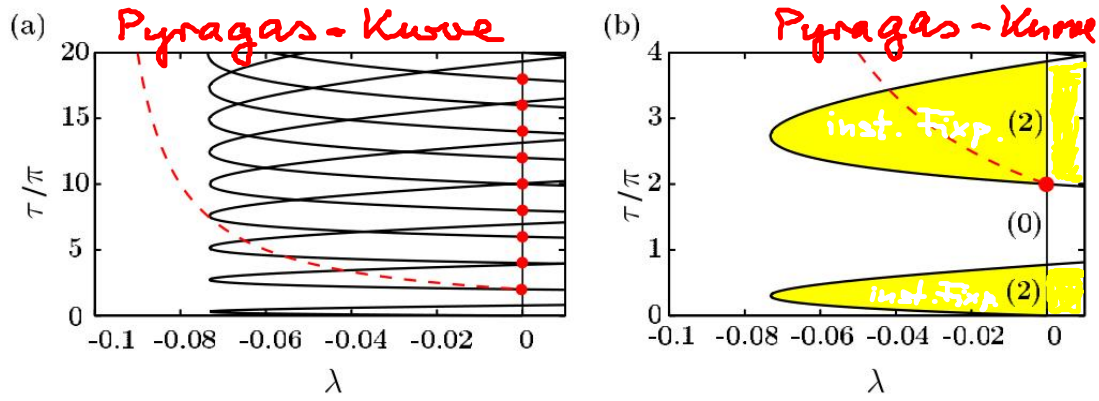

Fiedler et al PRL (2007)

FIG. 1 (color online). Pyragas (red dashed) and Hopf (black solid) curves in the (λ, τ) plane: (a) Hopf bifurcation curves $n = 0, \ldots, 10$, (b) Hopf bifurcation curves $n = 0, 1$ in an enlarged scale. Yellow (light gray) shading marks the domains of unstable $z = 0$ and numbers in parentheses denote the dimension of the unstable manifold of $z = 0$ ($\gamma = -10$, $b_0 = 0.3$, and $\beta = \pi/4$).

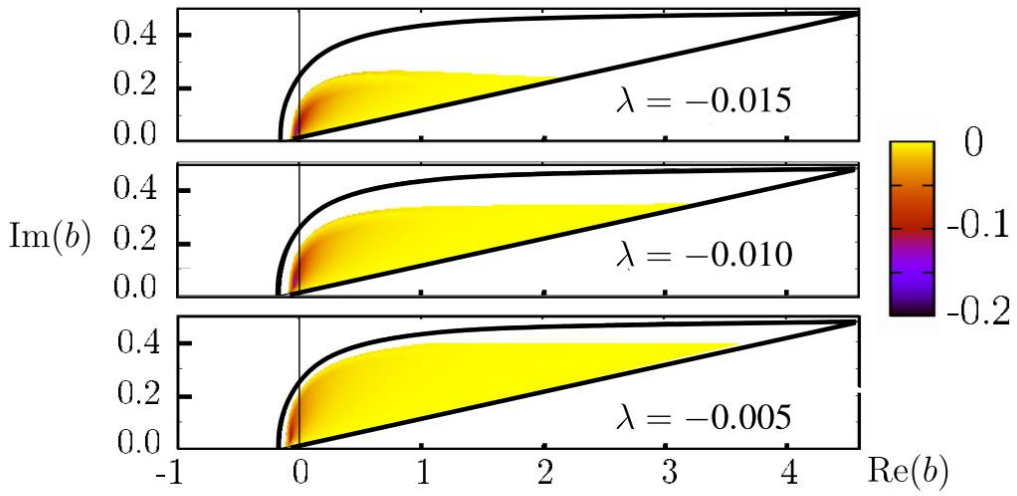

FIG. 3 (color online). Domain of control in the plane of the complex feedback gain $b = b_0 e^{i\beta}$ for three different values of the bifurcation parameter λ. The black solid curves indicate the boundary of stability in the limit $\lambda \nearrow 0$; see (18) and (19). The color-shading shows the magnitude of the largest (negative) real part of the Floquet exponents of the periodic orbit ($\gamma = -10$, $\tau = \frac{2\pi}{1-\gamma\lambda}$).

analyt. Bed.
$r_{Hopf}(\lambda) < r_{pyragas}(\lambda)$

Koppl. phase $\beta \neq 0$!

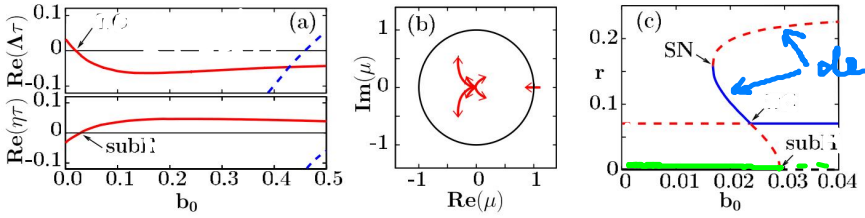

FIG. 2 (color online). (a) Top: Real part of Floquet exponents Λ of the periodic orbit vs feedback amplitude b_0. Bottom: Real part of eigenvalue η of the steady state vs feedback amplitude b_0. (b) Floquet multipliers $\mu = \exp(\Lambda\tau)$ in the complex plane with the feedback amplitude $b_0 \in [0, 0.3]$ as a parameter. (c) Radii of periodic orbits. Solid (dashed) lines correspond to stable (unstable) orbits. ($\lambda = -0.005$, $\gamma = -10$, $\tau = \frac{2\pi}{1-\gamma\lambda}$, $\beta = \pi/4$).

3.2.3 Chaos-Kontrolle durch zeitverzögerte Rückkopplung

Pyragas, Phys. Lett. A 170, 421 (1992):

$$\dot{x} = f(x) + KA\,[x(t-\tau) - x(t)] \qquad x \in \mathbb{R}^n,\ n \times n \text{ Kopplungsmatrix } A$$

$\dot{x} = f(x)$: chaot. Attraktor mit unendl. vielen UPO
→ s. Kap. 2

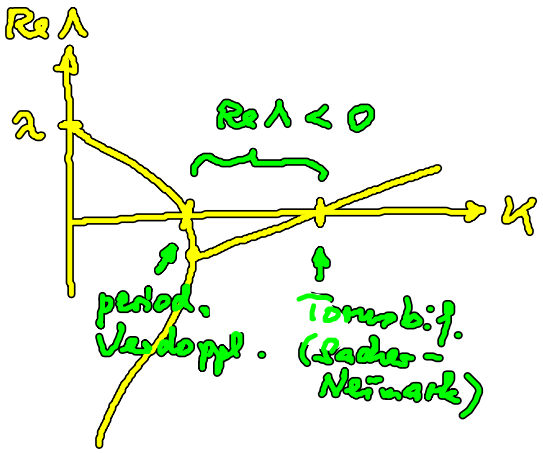

unkontr. Floquet-Problem:

$$\delta x = e^{\lambda t} u(t) \quad : \quad = u(t+T)$$

$$(\lambda + i\omega)u + \dot{u} = Df\,u$$

kontr. (diagonale Kontrolle):

$$\lambda u + \dot{u} = Df\,u + K(e^{-\lambda\tau} - 1)u$$

Just ⇒

$$\boxed{\lambda + K(1 - e^{-\lambda\tau}) = \lambda + i\omega}$$

Schöll u. Schuster (eds.): Handbook of Chaos Control (2008)

3.2.4 Kontrolle raum-zeitl. Systeme

Kyrychko, Blyuss, Hogan, Schöll: Chaos 19, 043126 (2009)

gray-Scott-Modell (Reaktions-Diff-System)

$$\begin{pmatrix} \dot{u} \\ \dot{v} \end{pmatrix} = \begin{pmatrix} -uv^2 + a(1-u) + D_u \nabla_u^2 \\ uv^2 - (a+b)v + D_v \nabla_v^2 \end{pmatrix} + KA \begin{pmatrix} u(t-\tau) - u(t) \\ v(t-\tau) - v(t) \end{pmatrix}$$

Aktivator u
Inhibitor v

3 räuml.-hom. Fixpkte

Aktivator-Kontrolle $A = \begin{pmatrix} 1 & 0 \\ 0 & 0 \end{pmatrix}$

Inhibitor-Kontrolle $A = \begin{pmatrix} 0 & 0 \\ 0 & 1 \end{pmatrix}$

- je nach Kopplungsschema (A), Delay-Zeit(τ) und Kontrollstärke (K) sowie Vorzeichen von K können verschiedene Raum-Zeit-Muster stabilisiert werden:

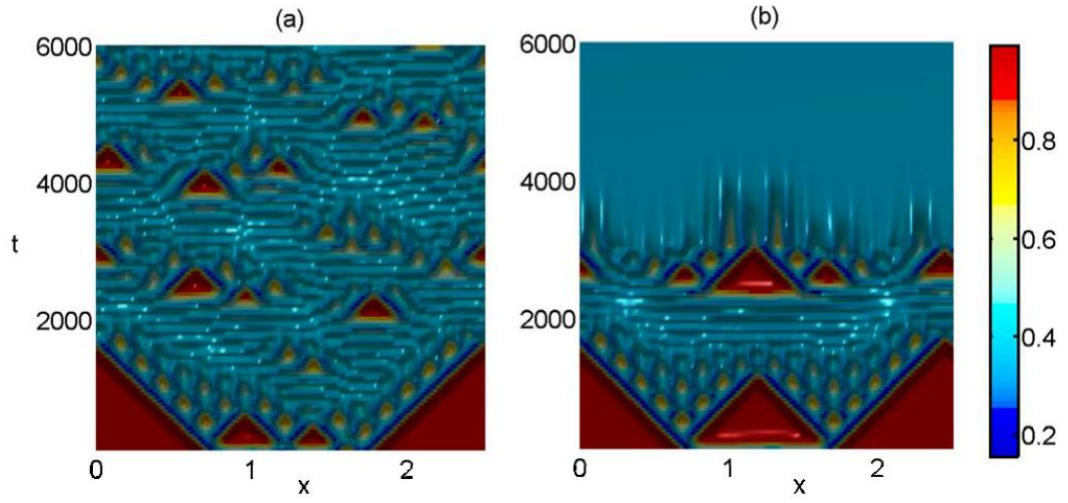

FIG. 4. (Color online) Space-time plot in the case of activator control. (a) Spatiotemporal chaos. (b) Nontrivial steady state E_1. The color code corresponds to the values of $u(x,t)$. Parameter values are $a=0.028$, $b=0.053$, $D_u=2\times10^{-5}$, $D_v=10^{-5}$, (a) $K=-0.4$, $\tau=0.1$ and (b) $K=-0.8$, $\tau=0.6$. Control is switched on at $t=3000$.

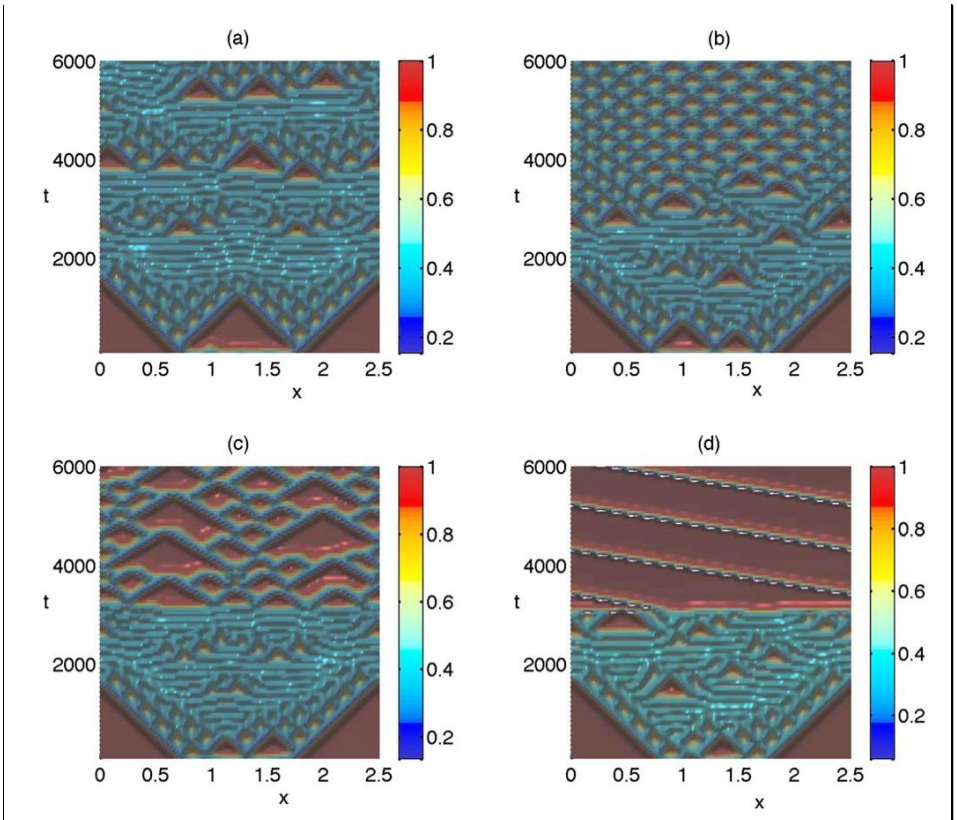

FIG. 5. (Color online) Space-time plot in the case of inhibitor control. (a) Spatiotemporal chaos. (b) Mixed (Turing–Hopf) mode. (c) Coarsening. (d) Transition to traveling waves. Parameter values are $a=0.028$, $b=0.053$, $D_u=2\times10^{-5}$, $D_v=10^{-5}$, (a) $K=-0.05$, $\tau=0.3$, (b) $K=-0.3$, $\tau=0.35$, (c) $K=-0.4$, $\tau=0.4$, and (d) $K=-0.6$, $\tau=0.75$. Control is switched on at $t=3000$.

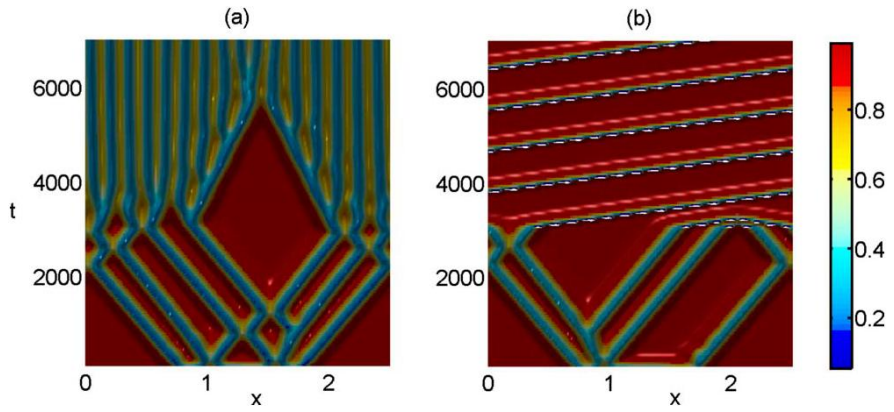

FIG. 7. (Color online) Space-time plot of control of traveling waves. (a) Activator control: Development of a stationary Turing pattern. (b) Inhibitor control: Transition to traveling wave. Parameter values are $a=0.022$, $b=0.053$, $D_u=2\times10^{-5}$, $D_v=10^{-5}$, (a) $K=-0.5$, $\tau=0.6$ and (b) $K=-0.8$, $\tau=0.4$. Control is switched on at $t=3000$.